

Hydropower intake-induced fish entrainment risk zone analysis

Mathew T. Langford, David Z. Zhu, Alf Leake, and Steven J. Cooke

Abstract: Evaluating the impacts of hydropower intake operations on upstream aquatic habitat is important for the development of environmentally sustainable hydropower and flood protection. A computational fluid dynamics model was used to simulate the flow field in the forebay of a high dam, Mica Dam in British Columbia, Canada. The model was used to evaluate the upstream hydraulics under various operational conditions and reservoir levels. This model, which was verified by a novel means of collected acoustic Doppler current profiler field measurements, highlights how appropriate intake selection may limit the volume of the forebay occupied by the entrainment risk zone. Additionally, a potential flow solution was applied to predict the velocity field induced by the intakes and the limitation of the potential flow solution was assessed. By linking the detailed knowledge developed of the forebay hydraulics to the established body of knowledge of fish behaviour, fish habitat use within the entrainment risk zone is also discussed in the context of hydropower optimization.

Key words: computational fluid dynamics, fish entrainment, hydropower, intake, reservoir forebay.

Résumé : L'évaluation des répercussions de la prise d'eau pour l'exploitation d'hydroélectricité sur l'habitat aquatique en amont est importante pour le développement d'une hydroélectricité durable sur le plan environnemental et la protection contre les inondations. Un modèle de la dynamique numérique des fluides a été utilisé pour simuler le champ d'écoulement dans le bassin d'admission d'un barrage élevé, soit le barrage Mica, en Colombie-Britannique, au Canada. Le modèle sert à évaluer l'hydraulique en amont dans diverses conditions d'exploitation et divers niveaux de réservoir. Ce modèle, qui a été vérifié au moyen d'une nouvelle méthode de mesure au moyen d'un professeur de courant à effet Doppler, met en évidence la façon dont la sélection appropriée de prise d'eau peut limiter le volume du bassin d'admission occupé par la zone de risque d'entraînement. De plus, une solution d'écoulement potentiel a été appliquée pour prédire le champ de vitesse induit par les prises d'eau et la limitation de la solution d'écoulement potentiel a été évaluée. En établissant un lien entre les connaissances détaillées sur l'hydraulique des bassins d'admission et les connaissances établies sur le comportement des poissons, l'utilisation de l'habitat des poissons dans la zone de risque d'entraînement est également examinée dans le contexte de l'optimisation de l'hydroélectricité. [Traduit par la Rédaction]

Mots-clés : dynamique numérique des fluides, entraînement des poissons, hydroélectricité, prise d'eau, bassin d'admission.

Introduction

The construction of high dams around the globe for flood protection and hydropower production has resulted in the impoundment of large rivers and thus the creation of deep reservoirs. Reservoirs create different thermal and flow characteristics relative to pre-impoundment riverine conditions that may lead to changes in fish assemblage as lotic-adapted species are replaced by lentic species (Liermann et al. 2012; Piria et al. 2019). Nonetheless, many reservoirs support vibrant recreational, commercial, and subsistence fisheries that contribute to livelihoods, economic development, and food security. For high head dams, where bi-directional fish passage is technically challenging or not feasible, upstream and downstream fish populations have limited connectivity (Schilt 2007). The normal feeding and rearing habits and basic movement ecology of fish upstream of dams may place them close to hydropower intakes at various times during the year, thus influencing entrainment risk (Coutant and Whitney 2000; Martins et al. 2013). Fish that become entrained — irrespective of fate — are removed from the reservoir population.

Fish entrainment has been identified as one of the key potential impacts of hydropower operations on the productivity and biodiversity of these aquatic species (Schilt 2007; Barnthouse 2013). Fish entrainment deals with a scenario in which fish in the upstream reservoir are involuntarily passed through water intake structures. Migratory fish are particularly susceptible to entrainment during downstream migration, but entrainment can also occur among resident fish using the habitat near the intakes (Coutant and Whitney 2000). It is anticipated that the risk of fish entrainment at a particular dam facility is associated with the effect of hydropower operations on the flow and thermal structure of the forebay as well as the biological characteristics of the resident fish population. Close to the intake, velocity becomes high, potentially exceeding the velocity at which fish are able to escape, thus resulting in fish entrainment into the intake units (EPRI 1992). This region is often termed the acceleration zone or the entrainment risk zone and its size can vary by species and life stage, which relate to swimming ability.

Received 22 July 2019. Accepted 12 January 2020.

M.T. Langford. Department of Civil and Environmental Engineering, University of Alberta, Edmonton, AB T6G 2W2, Canada; Canada Northwest Hydraulic Consultants Ltd., Edmonton, AB T6X 0E3, Canada.

D.Z. Zhu. Department of Civil and Environmental Engineering, University of Alberta, Edmonton, AB T6G 2W2, Canada.

A. Leake. Fish and Aquatic Issues, BC Hydro, Burnaby, Canada.

S.J. Cooke. Department of Biology, Carleton University, Ottawa, Canada.

Corresponding author: David Z. Zhu (email: dzhu@ualberta.ca).

Copyright remains with the author(s) or their institution(s). Permission for reuse (free in most cases) can be obtained from copyright.com.

Entrained fish mortality can be caused by shear stresses, pressure gradient, turbulence, cavitation or direct impact of turbine blades (Marcy et al. 1978; BC Hydro 2006a). Previous work has examined the use of physical, acoustic, and lighting methods to repel fish from this high risk zone (NPP 2005). To assess the efficiency of these operational devices, prediction of the near-intake velocity field upstream of the dam is necessary. Factors such as water velocity, temperature, depth, and acceleration affect the behaviour and distribution of fish. Hence, the flow pattern in the forebay area can provide valuable information on explaining fish movement and entrainment risk (Goodwin et al. 2006; Martins et al. 2014).

To assess the extents of the risk zone induced by the intakes, it is important that the upstream hydraulics are accurately characterized. Shammaa et al. (2005) explored developing an analytical potential flow solution to describe the flow upstream of orifices, which provides a base point for describing the flow upstream of hydropower facilities. Bryant et al. (2008) investigated flow upstream of orifices in a laboratory setting, including the impacts of multiple outlets, and proposed a modified potential flow solution. Huang et al. (2015) used a potential flow solution in combination with a physical model and computational fluid dynamic (CFD) solver to investigate the flow field upstream of the Baihetan dam, a high head dam in China. CFD solvers have been used for about a decade to generate flow fields upstream of hydropower facilities. Among them, the CFD studies of the Wanapum dam (Meselhe and Odgaard 1998), Dalles dam (Khan et al. 2004), Bonneville powerhouse (Rakowski et al. 2002), and Howard Hanson dam (Wicklein et al. 2002) are notable. On several occasions, CFD data was compared with physical model data and its reliability was ascertained (Meselhe and Odgaard 1998).

Large hydropower facilities may have deep reservoirs (>10 m) that have distinctly different thermal characteristics over the course of the year. The vertical density distribution of a thermally stratified water body may limit the elevation from which water is withdrawn. This phenomenon applies directly to hydropower intakes in thermally stratified reservoirs; it is called selective withdrawal (Fischer et al. 1979; Imberger 1980). Selective withdrawal is most common in reservoirs that have a very distinct thermal stratification profile (i.e., a sharp thermocline). The research of Shammaa and Zhu (2010) included a laboratory component to determine how total discharge through an orifice affects the proportion of withdrawal from each layer of a stratified water body. Several other studies also consider the concept of selective withdrawal and its impacts on upstream thermal stratification (Casamitjana et al. 2003; Caliskan and Elci 2009; Anohin et al. 2006; Islam and Zhu 2011).

The current study focuses on Mica dam upstream of the Columbia River, one of BC Hydro's largest generation facilities. The dam is a 244 m high concrete and earth-filled structure and was built primarily for flood protection as part of the Columbia River Treaty, however it is also a major producer of hydroelectric power. At the time of the field measurements, the dam was equipped with four Francis turbines, having a combined maximum generating capacity of 1740 MW. The dam has recently undergone expansion to include two additional turbines. Each of the six intakes is 12.7 m wide by 13.6 m tall at the dam's head wall and is separated by 21.4 m (centre to centre). The intakes at Mica are located at a geodetic elevation of 692.46 m. Intake 1 is the easternmost intake and Intake 6 is the westernmost intake (Fig. 1a). There are concrete wing walls located a distance of 8.9 m on either side of Intakes 1 and 6 (measured from the edge of the intake to the wing wall). The wing walls are both 12.2 m tall. The hydropower reservoir impounded by Mica dam, Kinbasket Reservoir, has a level that seasonally fluctuates depending on dam operations. In general, the reservoir level fluctuates by

approximately 25 m annually with the lowest pool elevations in May and the highest pool elevations in September.

BC Hydro has an ongoing ecological productivity monitoring program for a number of its large reservoirs including Kinbasket Reservoir for which fish population and thermal stratification of the reservoir are monitored (Bray et al. 2013). The 2008–2010 ecological productivity monitoring programs confirm that in the summer months there is significant thermal stratification throughout the reservoir (Bray et al. 2013). BC Hydro (2006b) indicates that the average fish of kokanee (*Oncorhynchus nerka*) is approximately 400 fish/ha in the vicinity of Mica dam, and that the distribution of fish in late summer ranges from 710 to 750 m geodetic elevation, with the majority of fish detections in the 730–735 m range. Kokanee is the most abundant sportfish species in Kinbasket Reservoir. This risk screening report identified that all life stages of kokanee are at high risk for entrainment as they frequently use the forebay adjacent to the intakes. Additionally, bull trout (*Salvelinus confluentus*), which prey on kokanee during their sub-adult and adult life phases, have been identified to be at risk of entrainment late in the year, when they make more frequent use of the forebay area just upstream of the dam (Martins et al. 2013). As such, highest risk scenarios for bull trout entrainment is during late fall and winter when the reservoir is isothermal.

To assess the entrainment risk to fish posed by the operation of the Mica facility, we conducted a study to analyze the upstream flow field of the reservoir under various operational conditions. This assessment was completed through a combination of acoustic Doppler current profiler (ADCP) measurements and CFD modelling. A CFD model was developed to simulate the flow field upstream of Mica under the field measurement scenario for the purpose of model verification. The model was subsequently used to evaluate the reservoir flow field during various operational scenarios, a useful approach to assess the relationship between fish swimming capability and various flow parameters. Both near-intake (within 50 m) and far-intake (1 km) flow fields were analyzed. The near-intake flow field is useful for demarcating the risk zone. The far-intake flow field may help to establish relationships between fish behaviour and characteristics of the flow field. The model result can also assist the hydropower producer in optimizing the operation of the facility to reduce entrainment related fish mortality. In addition to the field scenario, four additional scenarios were evaluated using the CFD model with various operational scenarios (Table 1). Each of these operational scenarios occur when the reservoir is isothermal as bull trout entrainment has been noted to be most significant during this timeframe (Martins et al. 2014), and it is anticipated kokanee entrainment is also greatest in these conditions (BC Hydro 2006b). The scenarios have been specifically selected to allow investigation of two objectives. The first objective is to investigate the effect of reservoir surface elevation on the flow field upstream of the dam, and the second objective is to investigate how the number of intakes that are operational affects the upstream hydraulics.

This study demonstrates a successful technique of completing challenging ADCP measurements in a deep, low velocity, lentic environment, investigates the impact of water surface elevation and intake withdrawal scenarios on the upstream hydraulics of the facility, identifies the extent of the risk zone under various operational conditions, and relates the knowledge gained about the forebay hydraulics to the potential for entrainment of resident fish. Additionally, this study evaluates the capabilities and limitations of CFD modelling and potential flow analysis in evaluating the flow field upstream of hydropower facilities.

Methodology

Field measurements

Field measurements of the reservoirs thermal structure were completed over a duration of six and a half months, and flow

Fig. 1. (a) Field measurement locations and (b) CFD model extents (2.5 km upstream of dam). [Colour online.]

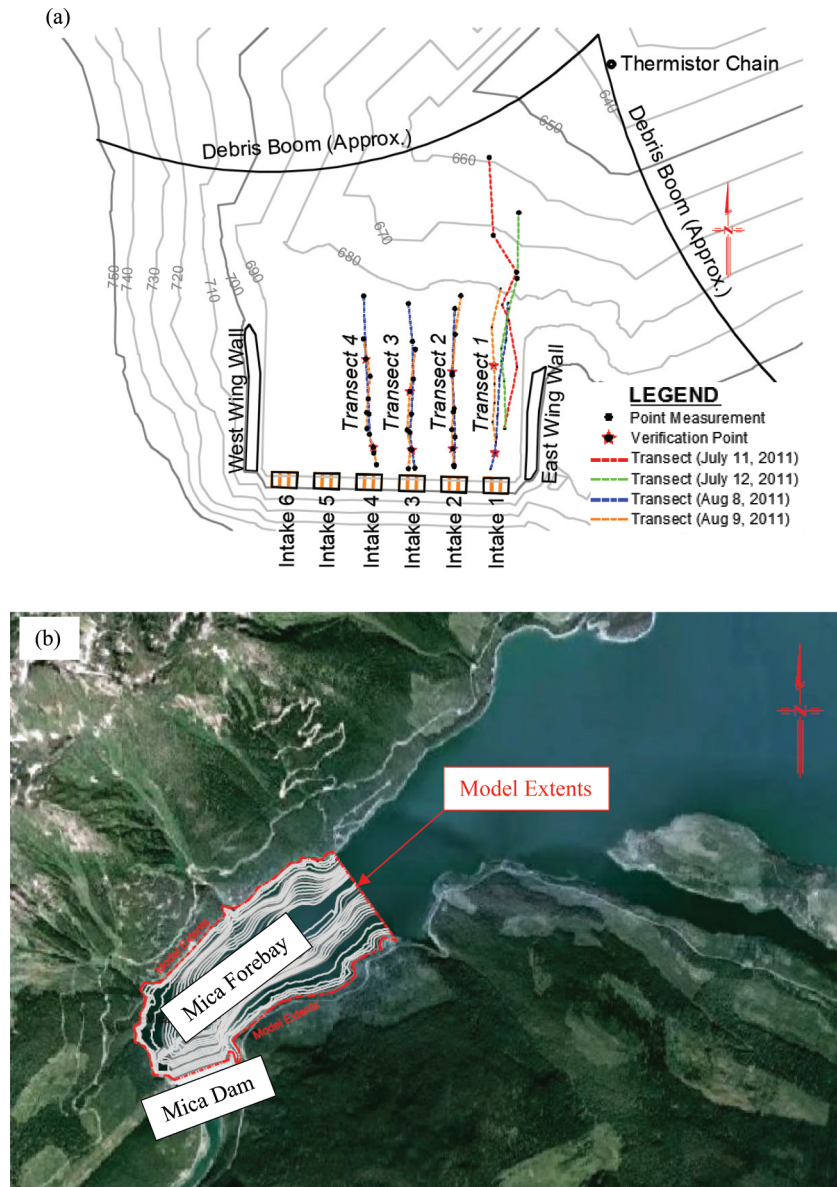


Table 1. Model scenarios.

Scenario	Description	Intake 1 (m ³ /s)	Intake 2 (m ³ /s)	Intake 3 (m ³ /s)	Intake 4 (m ³ /s)	Intake 5 (m ³ /s)	Intake 6 (m ³ /s)	Total Q (m ³ /s)	Water surface elevation (m)
Field	Field scenario	267	267	270	268	0.00	0.00	1072	752.98
A	Low head, 6 turbines	224	224	224	224	224	224	1344	726.55
B	High head, 6 turbines	224	224	224	224	224	224	1344	749.77
C	Low head, 4 turbines	215	217	235	234	0	0	901	726.55
D	Low head, 1 turbine	0	0	217	0	0	0	217	725.49

field measurements were completed during six days in July and August in 2011. Continuous temperature profile measurements were taken from May 13 to November 3, 2011 using a fabricated thermistor chain installed in the forebay close to the dam face, as shown in Fig. 1a. The Onset Tidbit v2 thermistors have an accuracy of 0.2 °C and read to a resolution of 0.02 °C. A total of 36 thermistors were spaced at approximately 2 m intervals along the depth of the chain starting 2 m below the water surface. Each of the thermistors collected data at 5 min intervals. The thermistor

measurements have been used to establish a thermal profile for the CFD model in this study.

Velocity profiles were measured during the two weeks of on-site field studies from July 11–13 and August 8–10, 2011 using an acoustic Doppler current profiler (ADCP) from a boat in the forebay. The Teledyne RD Instruments Workhorse Sentinel 600 kHz (Sentinel) was used. The locations of the ADCP measurements are shown in Fig. 1a. Each of the transects were oriented approximately perpendicular to the dam face and the location of each

stationary measurement ranges from 8 to 92 m upstream of the intake centre. The Sentinel has an accuracy of 0.3% of the water velocity relative to the instruments, or 3.0 mm/s and a resolution of 1 mm/s. The Sentinel has a beam angle of 20°, which restricts the approach distance the measurements can be made from the dam face. Velocity profiles in the immediate forebay were recorded when the dam spilling rates were held relatively constant throughout each measurement set (i.e., one or four transects). Several different discharges (63–274 m³/s) and two different operational scenarios (one intake versus all four intakes) were occurring during these measurement sets. During the July 2011 field work, measurements in front of Intake 1 were completed at discharges of 63 m³/s and 221 m³/s. During the August 2011 field work, measurements in front of Intakes 1–4 were completed at discharges of 240, 245, 270, 269 m³/s, respectively, the first day, and 252, 269, 274, 266 m³/s, respectively, the second day. ADCP measurements were particularly difficult at this facility due to the large depth of the forebay in the late summer, and restricted access to the banks of the forebay.

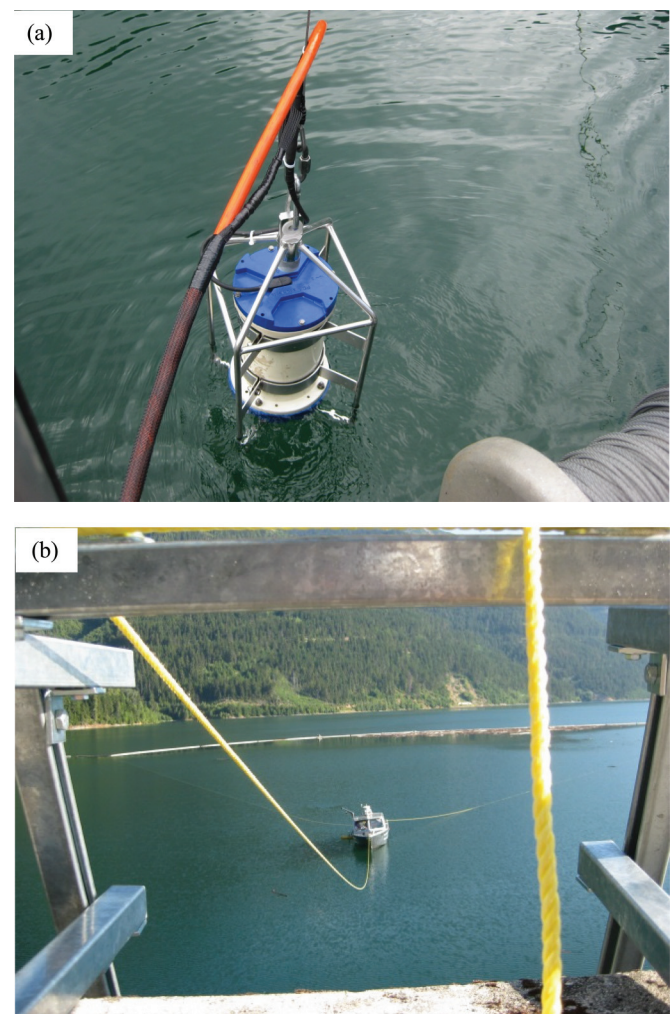
The reservoir level was approximately 61 m and 67 m above the intakes' centre during the 2011 July and August field studies, respectively. As the intakes are located at the base of the dam face, far from the water surface, it was determined that velocities are likely only significant close to the intakes and are of little significance high above the intakes. Therefore, to collect a more detailed view of the area of interest, the Sentinel was placed in a mooring cage and submerged between 20 and 35 m using the boat's hydraulic winch system, as shown in Fig. 2a. This set-up allowed the instrument to have a 0.5 m bin size while still reaching the bottom of the reservoir, where the intakes are located. In this orientation, the ADCP was able to collect measurements within the lowest 30–40 m of the water column, typically from the invert of the intakes to approximately 20 m above the top of the intake port.

Velocity measurement sets included either one (July measurements) or four transects (August measurements), approximately perpendicular to each operating intake on the dam face. Measurements were collected for a duration of 5 min at each point of interest. This extended measurement collection period allowed for time-averaging of the data during the post processing to reduce the error inherent to measuring relatively low velocity flow fields. The ADCP was tested in the field prior to collecting measurements to determine that 5 min allowed collection of enough measurements so that subsequent time-averaging of the values was not impacted by the number of measurements.

The physical location of each measurement was determined using a real-time kinematic global positioning system (RTK GPS), a Trimble R8 GNSS (Model 2). For stationary measurements, the rover was fixed on a trimaran boat, which was floating directly above the submerged ADCP transducer head. A base station was set up on top of the left bank, using a self-established benchmark. The location of this benchmark was checked against several benchmarks that were located on the dam structure (GCM #73C091, BM2500–2503, BM2248–2251). For kinematic surveying, this unit has a vertical accuracy of 20 mm and a horizontal accuracy of 20 mm.

There are a number of factors that can contribute to the potential error in ADCP measurements. Error may be introduced into the measurements when the ADCP is not perfectly horizontal due to boat movement. This is reflected in the pitch and the roll of the measurements. In general, minimizing the pitch and roll of the instrument is required for higher quality data. During field measurements, the water was relatively calm and the absolute pitch was maintained below 0.9° and the absolute roll below 1.1° (based on averaged data). On average, the pitch was approximately 0.3° and the roll was approximately 0.5°, which was deemed to be adequate.

Fig. 2. Field measurement setup: (a) inline mooring cage and (b) three point anchoring system. [Colour online.]



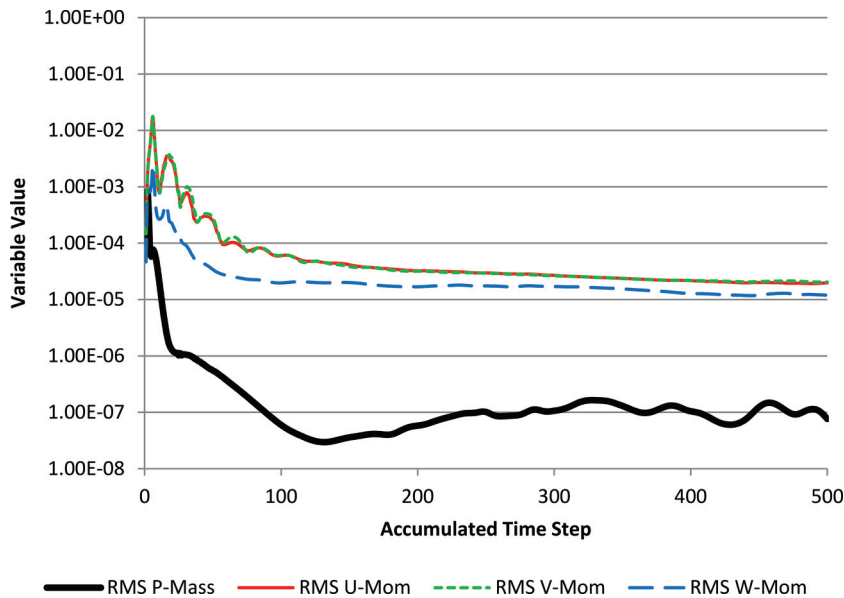
The relatively low flow velocity in lakes and reservoirs also contributes to potential flow field measurement error, which requires averaging of stationary measurements. The ADCP can drift over the course of each stationary measurement, which is difficult to control. Drifting contributes to error in the measurements during post-processing. During the July field trip, only two anchoring lines were used to secure the boat resulting in substantial drift during velocity measurements. Therefore, for the August field trip, the data collection procedures were revised to include a third anchoring line, which greatly reduced the drift of the ADCP as shown in Fig. 2b. For the measurements in July, each stationary point had a horizontal drift contained to an average radius of 3.9 m. Measurements in August were much more stationary, with horizontal drift contained to an average radius of 0.4 m for each point. Due to the increased potential for error in the July field measurements, the July measurements were not used in this study.

As previously mentioned, at each point measurement location, measurements were recorded for approximately 5 min collecting about 150 velocity profiles. These measurements were later averaged to reduce the error due to this dynamic behaviour.

CFD model development

CFD modelling for this study was completed using a commercially available solver, Ansys CFX. The extent of the CFD model of

Fig. 3. Convergence history of the governing equations. [Colour online.]



the Mica forebay cover the forebay extending from the dam face to approximately 2.5 km upstream as shown in Fig. 1b. While the impacts of the hydropower intakes are hydraulically relatively localized, the larger model domain allows to model to better represent broader physical phenomenon such as thermal stratification. The CFD solver uses the three-dimensional Reynolds-averaged Navier-Stokes equations, with the $k-\varepsilon$ turbulence model to assess eddy viscosity. The $k-\varepsilon$ model was selected for its robustness and excellent numerical stability, in addition to the fact the severe pressure gradients were not anticipated. To compute mass transport, a full buoyancy model was chosen. Density profiles for the computed temperature profiles were determined using an equation of state. The computed density was then substituted into the Navier-Stokes equations to compute the buoyancy source term.

The model boundaries were constructed using a patch conforming tetrahedral mesh. The model's bathymetry was created using topographic information provided by BC Hydro. The upstream bathymetry is generally constructed from pre-flooding contours of the upstream river basin, dated 1954. The contours have a spacing of 30.48 m (100 ft.). The banks (for geodetic elevations greater than 714.5 m), have some bathymetry refinement, based on information dated 2002. This information is stereophotographic information and has a general lateral spacing of 15 m \times 15 m. The hydropower intakes, wing walls, upstream apron, and other dam details were constructed utilizing record drawings dated 1989.

A free-slip wall boundary was used at the reservoir's free surface, while other walls were modelled using no-slip conditions, where the standard wall function was used. At the Mica intakes, mass-flow rate boundary conditions were provided. At the upstream boundary, an 'opening' boundary was provided, allowing both inflow and outflow across the boundary.

Mesh independence was investigated using three different mesh sizes. The edge length of the coarse mesh (Mesh 1) was the default length determined by the meshing software (Ansys Meshing). Two finer meshes were constructed by systematically reducing the edge length of the elements in the mesh. The second intermediate mesh (Mesh 2) had an edge length of 0.5 times the edge length of Mesh 1. The finest mesh (Mesh 3) had an edge length of 0.5 times the edge length of Mesh 2. In evaluating the performance of each mesh it was determined that the average discrepancy between Mesh 1 and Mesh 2 was 5.4%, with a

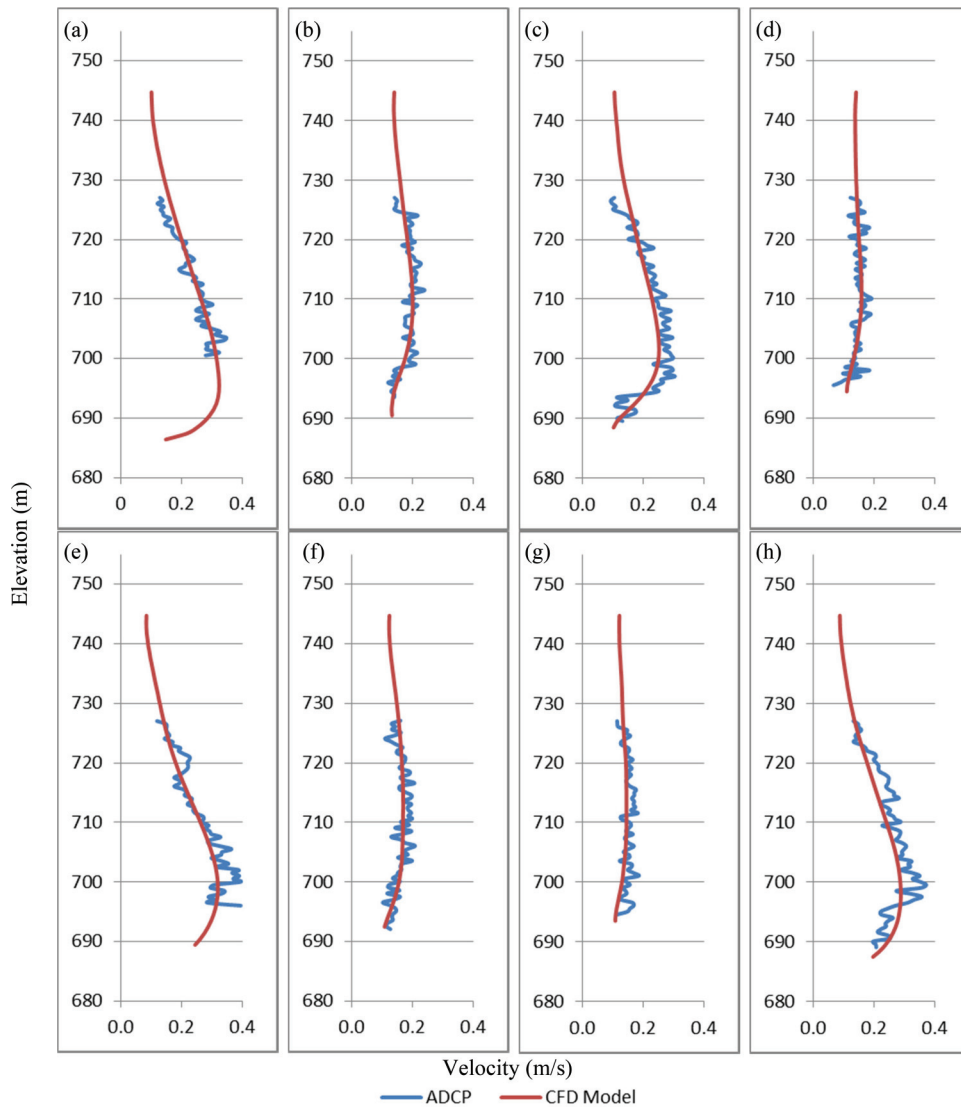
maximum discrepancy of 10.3%. The average discrepancy between Mesh 2 and Mesh 3 was 0.6%, with a maximum discrepancy of 1.9%. Based on these discrepancies, we determined that Mesh 2 was the appropriate mesh to use for the completion of this study, which minimizes uncertainty due to mesh size, while maximizing computational efficiency.

In total, the entire model domain includes 4.6 million nodes for the chosen mesh size (Mesh 2), arranged in an unstructured tetrahedral mesh. Some local refinement of the computational mesh was required in proximity to the intakes. This mesh refinement allows for more detailed modelling in this zone, which has higher velocity gradients, and is particularly important for fish entrainment risk assessment. This zone extends spherically from the intake centre to a radius of 200 m, extending beyond the debris boom. Within the refinement zone, a maximum element edge length of 1 m is specified, which expands to 4.6 m at the edge of the refinement zone. The coarse mesh throughout the model domain has face sizes ranging from 4.6 to 50 m depending on the location and proximity to boundaries. The mesh was developed using a three-step adaptive meshing procedure, which introduces additional elements in regions within the domain with higher numerical instability. At the intakes, which are 12.7 m \times 13.6 m (height \times width) mesh elements range from 0.1 to 0.45 m in size.

The convergence criteria for the model were set such that the root mean square (RMS) of the residual is below 10^{-4} in all the simulations carried out. Figure 3 shows a typical convergence history for the momentum and the pressure equations, demonstrating excellent convergence.

During the field measurements collected at Mica, the forebay was found to be thermally stratified. The water temperature varied gradually to a depth of 62 m, where it became isothermal. To reflect thermal stratification in the verification run for the CFD model, the measured temperature profile of the reservoir was fit to an empirical equation. The temperatures that were fit to the equation were the average values measured at each depth over the course of the three days of velocity measurements (August 8 to 10, 2011). In this empirical equation, temperature T ($^{\circ}\text{C}$) at a given geodetic elevation Z (m) can be represented as a function of water depth D (m), where $D = 752.98 - Z$ with 752.98 being the average geodetic elevation of the water surface.

Fig. 4. Model verification — velocity magnitude at specific distance upstream of dam: (a) August 8 – Transect 1, 17.4 m; (b) August 9 – Transect 1, 61.5 m; (c) August 8 – Transect 2, 24.6 m; (d) August 9 – Transect 2, 57.1 m; (e) August 8 – Transect 3, 17.4 m; (f) August 9 – Transect 3, 46.9 m; (g) August 8 – Transect 4, 62.6 m; and (h) August 9 – Transect 4, 18.1 m. [Colour online.]



$$(1) \quad T(Z) = \begin{cases} 2.3521 \times 10^{-6}D^4 - 3.0628 \times 10^{-4}D^3 + 1.3796 \times 10^{-2}D^2 - 4.621 \times 10^{-1}D + 18.374 & D < 62 \\ 4.47116 & D \geq 62 \end{cases}$$

The fitted curve has been separated into a piece-wise function, with the upper portion representing the gradually varying thermal stratification of the forebay and the lower portion representing the isothermal layer at the bottom of the water column. From the fitted temperature profile, density was computed based on the fluid properties of freshwater in the practical temperature range (Potter and Wiggert 2002). It was observed that the density–temperature variation can be fitted by the following equation:

$$(2) \quad \rho = -0.0057T^2 + 0.0234T + 999.87$$

where ρ (kg/m^3) is the density at a given point. This equation was supplied as the ‘equation of state’ in the CFX solver to get the density from the simulated temperature distribution.

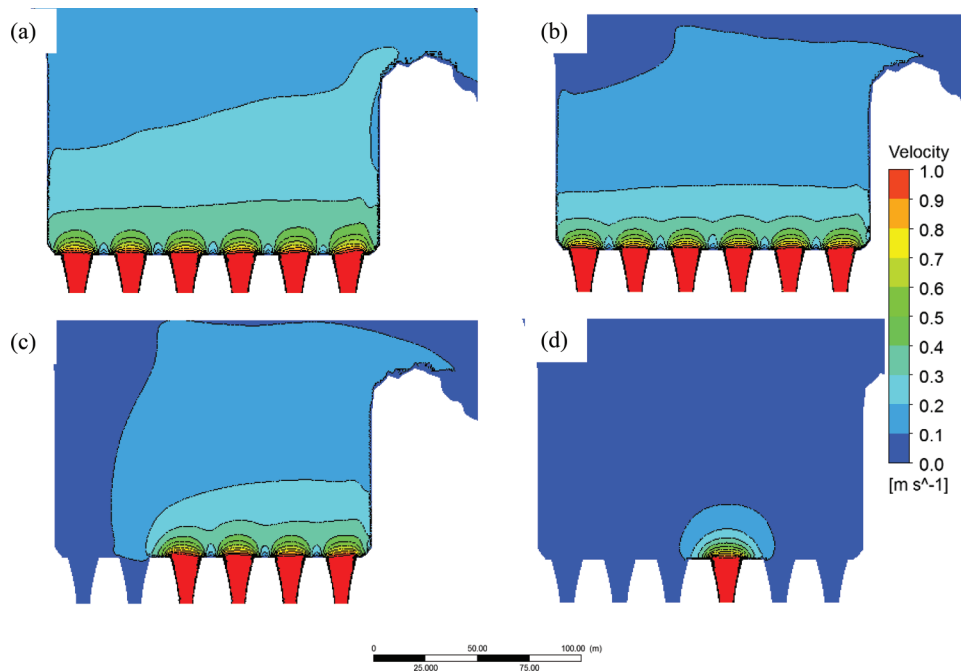
At the upstream boundary, it was required to calculate the static pressure for the given density profile by solving the following integration:

$$(3) \quad \int dP = \int (\rho - \rho_{\text{ref}}) g dZ$$

where P is the static pressure (Pa), ρ_{ref} (kg/m^3) is the density of water at surface, and g is -9.81 m/s^2 .

In addition to the field scenario, which was used to compare the model’s performance to the field measurements, various other scenarios were developed corresponding to operations in which tagged fish were in proximity to the dams’ intakes. Four select scenarios, capturing a broad range of operational scenarios in which fish entrainment was probable, are outlined in Table 1.

Fig. 5. Velocity at centre of intake elevation (692.46): (a) Scenario A, (b) Scenario B, (c) Scenario C, and (d) Scenario D. [Colour online.]



Each of these scenarios are isothermal, representing the operational scenarios that are most relevant for fish entrainment risk assessment.

Model verification

The results generated by the CFD model for the field scenario were compared against the field ADCP measurements conducted during the August field trip to verify the CFD model. Each of the velocity measurements completed at Mica were completed in duplicate, on separate days. The maximum difference measured between the two days was 0.43 m/s with average differences limited to 0.08 m/s across the domain where field measurements were completed. The model verification included comparing the CFD simulations to the field measurements by evaluating each of the three velocity components. Vertical velocity magnitude profiles for each of the measurements (noted by a star on Fig. 1a) is included as Fig. 4. Two measurements were completed along each transect, one for each of the two days that field measurements were conducted (for a total of eight comparisons on each transect). In general, the velocity magnitude ($(u^2 + v^2 + w^2)^{0.5}$), u velocity (toward to dam face), and w velocity (vertical) were fastest in the left hand, lower corner, where the intakes are located.

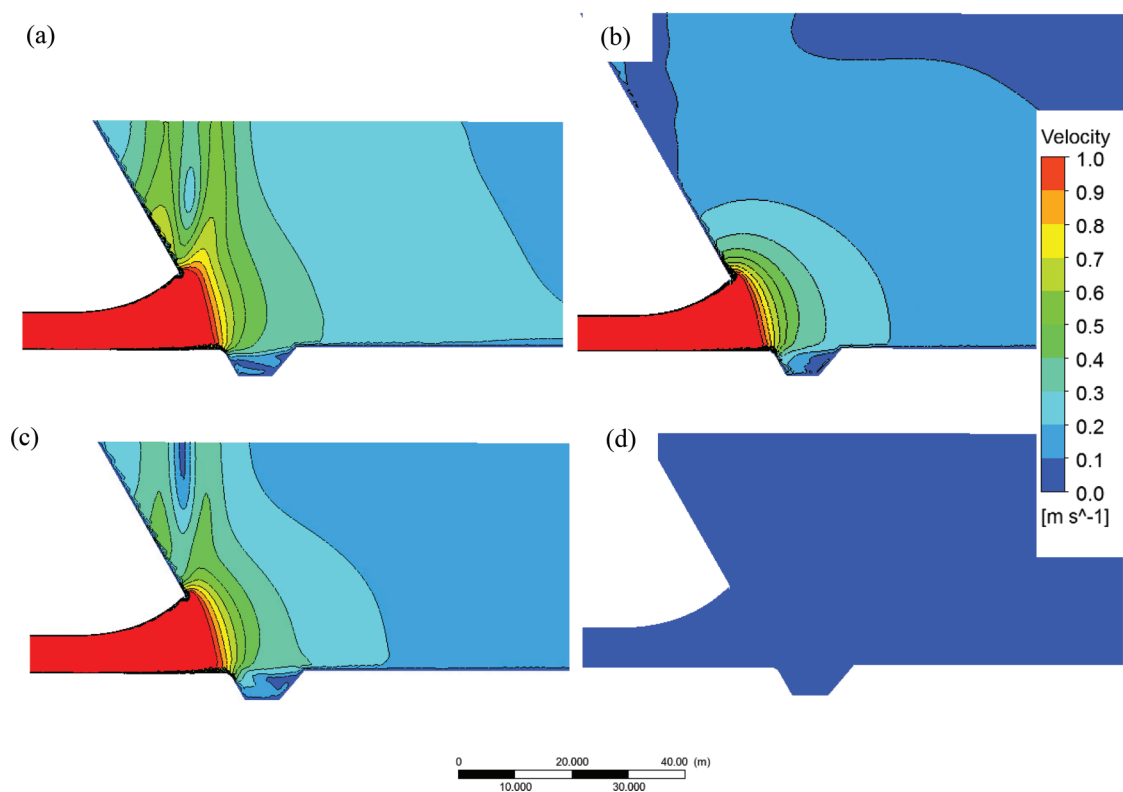
For the field measured velocities, the maximum velocity magnitude was approximately 0.5 m/s for the measurements located 15 m from the intakes. Transects 2 and 3 had faster velocities further from the intakes, which was due to the interaction of adjacent intakes. This trend is also seen in the u velocity measurements, where the maximum velocity was approximately -0.5 m/s (i.e., toward the dam face). z velocity contours had a maximum velocity of approximately -0.15 m/s (i.e., downward) but were in general much smaller than the u velocity contours, and v velocity (parallel to the dam face) followed the same trend on both sets of measurements. The v velocity was generally moving towards the left bank and getting progressively larger when moving from Transect 1 to 4. At Transect 1, the velocity was mostly negative (maximum 0.1 m/s) and generally flowing towards the right bank. Transect 4 had the largest v velocities, with a maximum of 0.25 m/s. These trends indicate a counterclockwise recirculation pattern at the right bank.

In general, the velocity magnitude and lateral velocity components (u and v) are predicted well by the model, with maximum discrepancies of 0.14 m/s perpendicular to the dam (x direction), 0.12 m/s parallel to the dam (y direction), and 0.16 m/s for overall velocity magnitude. The absolute mean discrepancy between the field measurements and the CFD model were 0.03 m/s (x direction), 0.04 m/s (y direction), 0.03 m/s (z direction), and 0.06 m/s (velocity magnitude). Both the pattern and the magnitude of these parameters match the measurements well. An example of the CFD simulated velocity magnitude profiles, compared to the field measured profiles, is included as Fig. 4. It can be noted that the location of the peak velocity matches well between the numerical simulation and the field measurements, although there is some discrepancy upstream of the zone of high velocity. The greatest discrepancy with the modelled results was consistently noted in the vertical velocity, in which the model over-predicts the downward velocity of water. The maximum discrepancy in this direction was 0.11 m/s, which is of similar magnitude to the two horizontal directions; however, the magnitude of the downward velocity is much lower than the lateral components, making the discrepancy comparatively larger. This discrepancy between the field measurements and CFD model is likely due to the field measurement uncertainties given the large depth of water at the intake location and the relative low flow velocity away from the intakes. Despite the fact that the ADCP was lowered to a depth of 20–35 m below the water surface, the size of the sampling volume was approximately 20 m wide at the bottom of the water column as the ADCP has a beam angle of 20°. We believe a relative error of 30% is acceptable as it indicates the reliability of both the field measurements and the CFD modelling.

Forebay flow field

The result of the CFD model of the Mica forebay was used to evaluate the impacts of various operational configurations on the upstream flow field. Specifically, hydraulic parameters that have been previously noted to potentially affect entrainment were investigated including velocity, turbulent kinetic energy, shear

Fig. 6. Velocity profile at Intake 1: (a) Scenario A, (b) Scenario B, (c) Scenario C, and (d) Scenario D. [Colour online.]



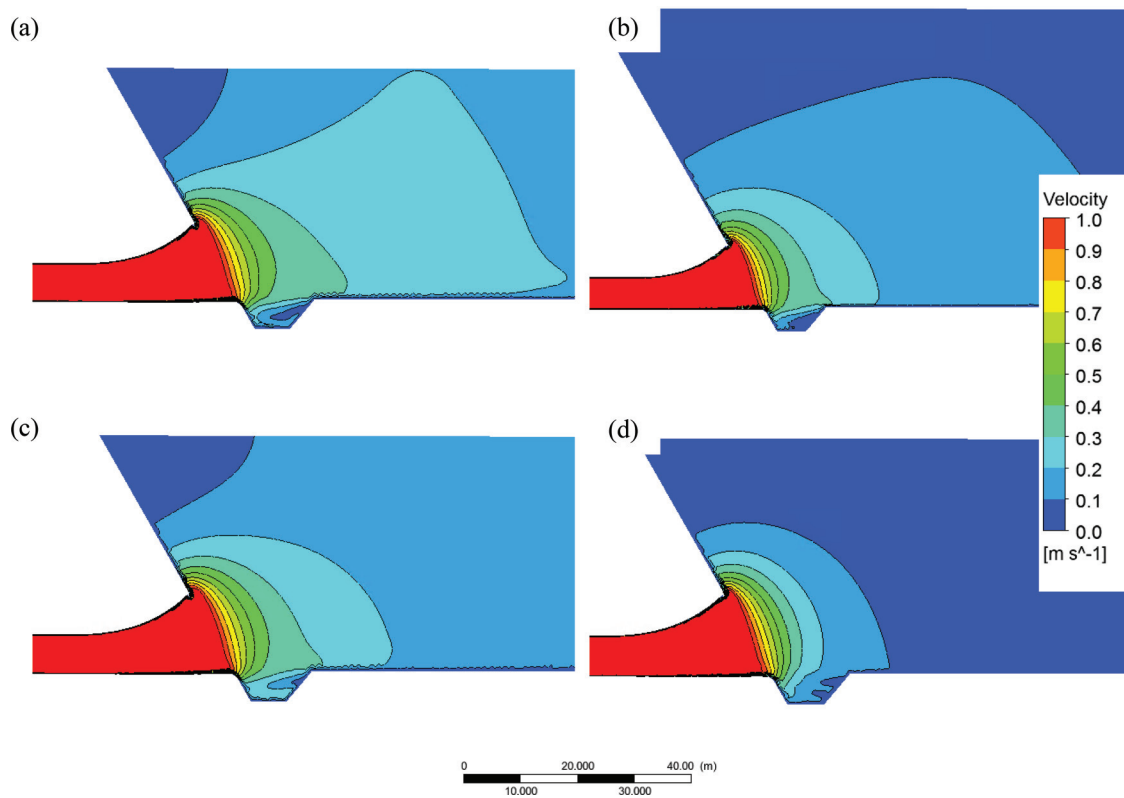
strain rate, and velocity curl (BC Hydro 2006a; Coutant and Whitney 2000; Goodwin 2004; Langford et al. 2015).

The velocity field that develops upstream of the intakes is shown in plan view (at the intake midline elevation) in Fig. 5. It can be noted that the zone of influence of the dam extends much further upstream of the dam depending on the number of intakes that are operational. In comparing the low pool scenarios (A, C, D, where the reservoirs elevation is approximately 35 m above the intakes' centre), the velocity contours in scenario A, when six turbines are operational, become parallel to the dam face within approximately 10 m of the dam face. Beyond this, the larger velocity field generated by the intakes spans the entire width of the forebay and the dam begins to act as a line sink, as opposed to series of point sinks. In scenario D, where a single unit is operational, the velocity contours are ellipsoidal in shape, extending away from the intake. In this scenario, the single operational intake acts as a point sink. When evaluating the impact of depth on the velocity field, it is noted that in the low pool scenario (A) the velocity field extends further upstream than in the high pool scenario (B). Fish that are occupying the forebay during low pool (late-winter to spring) at a depth close to the intakes could be exposed to higher velocities due to the difference in cross-sectional area approaching the intakes. It can be noted that generally the portion of the forebay that is impacted by higher velocities (>0.5 m/s) is localized around each intake for each scenario. There is, however, a distinct difference in the portion of the forebay that exceeds the swimming capability of resident fish if a lower threshold, such as 0.1 m/s, which may have implications for juvenile, anguilliform swimmers (Katapodis and Gervais 1991). The volume of the forebay exceeding 0.1 m/s increases substantially with the number of intakes operational as well as when the water surface elevation is lower. Thus, the threshold velocity for entrainment risk is largely dependent on the species of fish present in the reservoir and their life stage (Katapodis and Gervais 1991).

It is also of interest to evaluate the flow field generated by the intakes in profile view. Vertical velocity profiles extending perpendicular from the dam into the forebay upstream of Intakes 1 and 3 are shown for each of the four scenarios in Figs. 6 and 7, respectively. The velocity field upstream of Intake 1 demonstrate contours uniform velocity in the vertical direction in the low pool scenarios where 6 and 4 turbines are active (scenarios A and C). In these scenarios, fish may be exposed to higher velocities regardless of swimming depth during low pool in late winter and early spring. It can also be noted that there is a strong velocity field oriented above Intake 1 in these scenarios, where a vortex is generated, which is discussed further below. This phenomenon is not apparent in the high pool scenario (B), despite there being a large discharge through the dam. In this scenario the contours are ellipsoidal in shape. The impacts of the wing walls that are adjacent to Intake 1 and Intake 6 and other boundaries that may drive vortex formation and increase fish entrainment risk are reduced in high pool scenarios. At Intake 3, the velocity field has more ellipsoidal contours in all scenarios as shown in Fig. 7. As noted previously, the higher flow scenarios result in increased velocities when more intakes are active, which is especially prevalent in the scenarios with lower water surface elevation.

In scenarios A and B, where all intakes are operational, it was noted that the velocity field contour becomes parallel to the dam face a certain distance upstream, a point at which the flow field can be approximated as a line sink instead of a series of point sinks. Figures 8a, 8b and 8c show the velocity field degradation with distance at the intakes elevation, as well as 15 m and 30 m above the intake elevation respectively. At the intakes elevation (Fig. 8a), it can be noted that for all distance upstream, higher velocities are generated in the low pool scenario versus the high pool scenario. The difference in velocity between each of these scenarios becomes more distinct as distance from the intakes is increased, with almost two times the velocity simulated 50 m upstream of the intakes in the low pool scenario (A).

Fig. 7. Velocity profile at Intake 3: (a) Scenario A, (b) Scenario B, (c) Scenario C, and (d) Scenario D. [Colour online.]



The velocity field also undergoes a distinct transition from having an undulating nature, with distinct velocity difference at various distances across the dam face, to a more uniform nature further away from the dam. This transition happens at approximately 15 m upstream of the dam face. At an elevation 15 m above the intake elevation this same transition is still apparent. The increased velocity caused by the vortex is also noted within 10 m of the intakes for the low pool scenario (A). At 30 m above the intakes, the same pattern is still apparent. It can be noted that the velocity induced by the vortex in scenario A is not diminished with distance above the intake. This vortex creates a scenario in which the area located above Intake 1 and Intake 6 is of high risk for fish entrainment for all low pool scenarios when that intake is active.

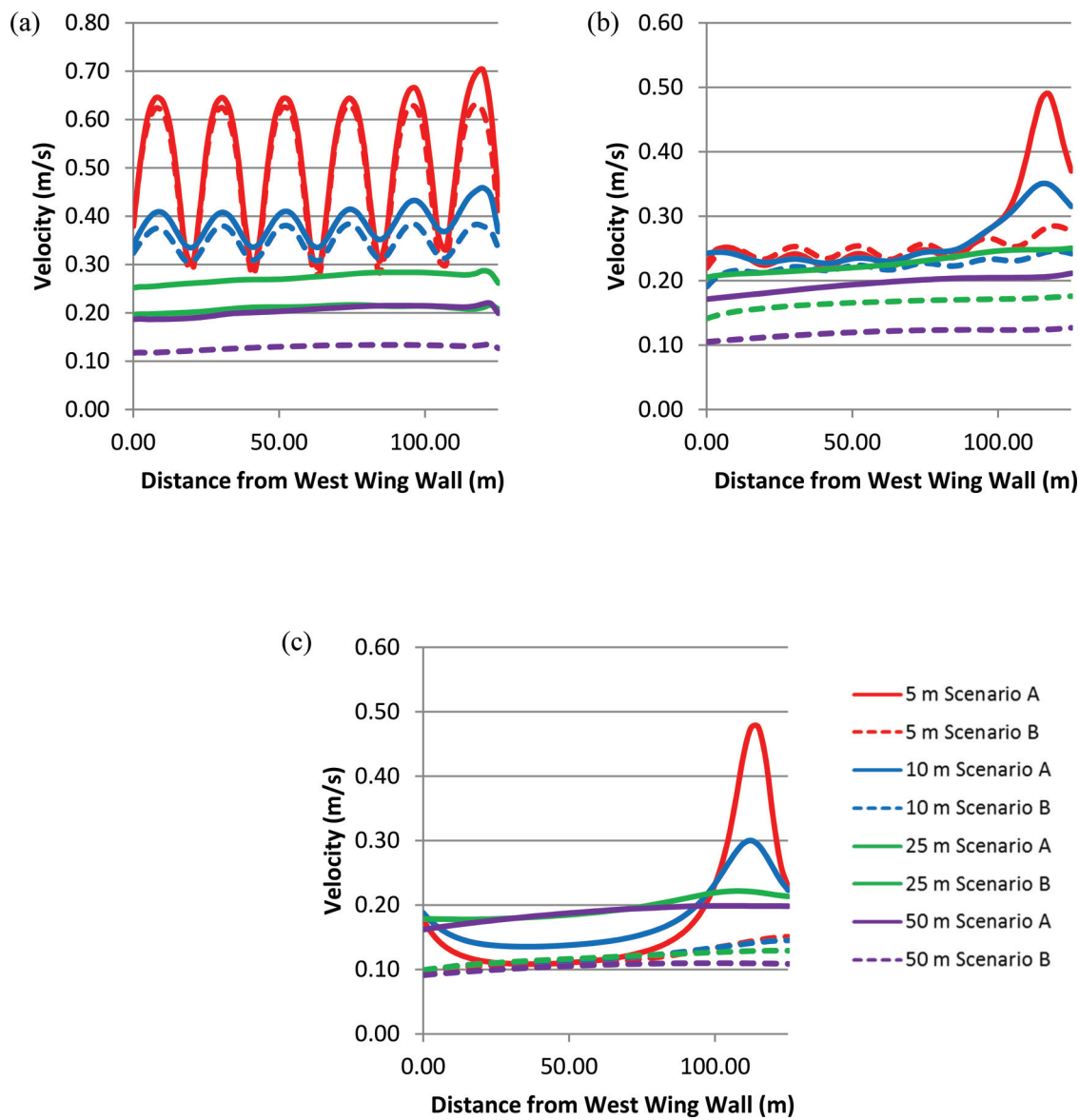
To evaluate the validity of using a more rudimentary model to evaluate the dam forebay flow field, the results of scenarios A and B were also compared with a potential flow solution following the approach of Huang et al. (2015). The potential flow solution was developed by superimposing the flow field generated by a series of single intakes to determine the flow field generated by six operational intakes. The reservoir bottom, side walls, and water surface were included in the potential flow solution by the inclusion of image intakes to simulate the impact of these boundaries. In the solution, 20 images were superimposed to represent both the side walls, as well as the water surface and reservoir bottom. The advantages of applying potential flow theory are that it is less computationally intensive than developing a CFD model.

The potential flow solution is compared to the averaged CFD model output upstream of each intake for scenarios A and B in Figs. 9a and 9b, respectively. It appears that the potential flow solution overestimates the magnitude of the peak velocities near the intakes. The potential flow solution describes the peak velocities directly in front of the intakes well for locations greater than 10 m upstream of the intakes. There is a greater discrepancy between this solution and the simulated flow field near the water

surface, which is because additional images (greater than 20) of the intakes were not included in the potential flow solution at the water surface. As such, the potential flow solution near the water surface more closely matches the CFD output for the deep reservoir scenario, as the mean velocity throughout the forebay in this scenario is lower. The potential flow solution also matches the CFD simulation better as distance upstream of the intakes increases. This better correlation is because the potential flow solution does not consider the unique hydraulic phenomena that were simulated near the dam face by the CFD model, including vortex formation. The rectangular geometry used in the potential flow solution does not accurately predict the impacts of the complex geometry near the dam structure. In general, the potential flow solution is capable of predicting the flow field for distances greater than 10 m upstream of the intakes (distances greater than approximately $1 \times$ the hydraulic diameter of the intake), however it does not represent near-intake flows accurately. As the potential flow solution is less computationally and time intensive than the numerical solution, it does provide valuable information of the forebay's flow characteristics for less detail-intensive applications.

The velocity profile upstream of the dam differs from intake to intake. Figure 10 identifies the change in velocity profile at various distances upstream of Intakes 1 and 3 simulated by the CFD model. In all scenarios, there is a distinct peak in velocity at the intakes' elevation in the water column at distances within 15 m of the intakes. This peak is most distinct in the high pool scenario, which indicated a great velocity gradient with depth. Beyond 15 m upstream of the intakes the velocity field become uniform with depth in all scenarios. As noted previously, in the low pool scenarios where Intake 1 is actively discharging water from the reservoir, much higher velocities (greater than 0.5 m/s) exist all the way to the water surface. It is also of interest to note that despite the presence of vortices above Intake 1, the potential flow analysis still yields satisfactory predictions, particularly

Fig. 8. Velocity magnitude at varying distances in front of the intakes for Scenarios A and B: (a) intake elevation (692.46 m), (b) 15 m above intake elevation (707.46 m), and (c) 30 m above intake elevation (707.46 m). [Colour online.]



regarding the location and magnitude of the peak velocity, which is not seen in front of Intake 3, which is further from the wing wall.

Isovolumes were produced using CFD to determine the volume of the forebay that exceed certain threshold velocities, which can be compared against fish swimming capabilities. The threshold limits that are evaluated in this study include 1.0, 0.5, 0.25, and 0.15 m/s. The volume of the forebay upstream of the dam headwall that is occupied by each of these isovolumes is presented in Table 2. In comparing the volume of water above the 0.15 m/s and 0.25 m/s threshold, it is apparent that both discharge through the dam and the water surface elevation play a prominent role in determining the flow field upstream of the dam, and thus, the risk volumes. The higher threshold, 0.5 m/s and 1.0 m/s, are less dependent on water surface elevation and generally are impacted by the volume of water passing the intakes.

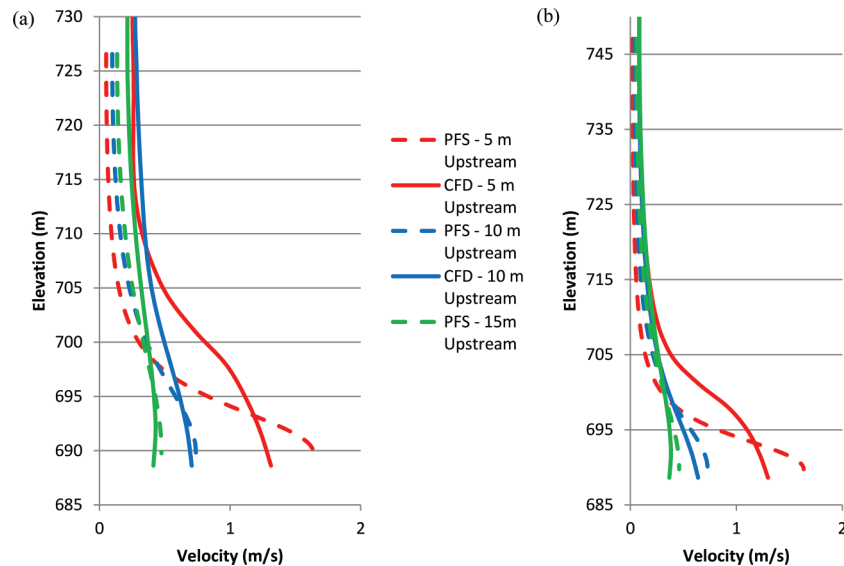
BC Hydro operators have noted a consistent surface-oriented vortex generated above Intake 1 during low pool. The velocity

curl, or vorticity, about the vertical axis that is generated by the boundaries is investigated in Fig. 11, which looks at the velocity curl on vertically oriented planes extending perpendicularly into the forebay from Intake 1. In scenarios A and C, when Intake 1 is active, and the water surface elevation is low, a vertical-axis core of high vorticity is generated. This vortex causes the swirling flow and downward velocity. When the water level is higher, despite having a high discharge, this vertical core is less apparent, and the peak values of velocity curl are less intense. Vorticity generation at Intakes 2–4 is less distinct, and vorticity is generated adjacent to the boundaries without establishing a vertical-axis core. These results indicate that the proximity of Intake 1 to the east wing wall is the primary driving force in the development of the vortex core.

Fish entrainment risk in a biological context

The volume of the high-risk zone for fish entrainment increases exponentially with decreasing threshold swimming speed. Thus,

Fig. 9. Potential flow solution versus CFD model velocity profiles: (a) Scenario A and (b) Scenario B. [Colour online.]



high-risk zone for weaker swimmers and thus, smaller and younger fish located in the forebay adjacent to the intakes is much greater than that of larger fish with greater swimming capabilities. Fish swimming capability at various life stages is a biological characteristic that impacts fish entrainment at hydropower facilities once fish are in the vicinity of turbine intakes. The work done by Katapodis and Gervais (1991) suggests that swimming capability is largely a function of fish size and body form and swimming style. Typically, salmonids, which exhibit subcarangiform swimming style, have sustained swimming capabilities of between 0.5 and 1.0 m/s depending on body length. Juvenile fish, with body lengths less than 200 mm may also be at risk of entrainment at velocities below 0.5 m/s. The swimming curve developed by Katapodis and Gervais (1991) suggest that for Kinbasket kokanee, which are generally 200–300 mm in length at maturity (Bray et al. 2013), and are subcarangiform swimmers, translate to swimming burst distances ranging from 2 to 5 m in water velocities greater than 1 m/s, which may not be sufficient to escape the high-risk zone for entrainment. Velocities below 0.5 m/s however can be sustained by the species for a long period of time for these adult fish. The threshold for smaller fish has yet to be established but will most certainly be lower than the value for adult fish, which may suggest that early life stages of kokanee could be at particular risk of entrainment if they encounter the forebay region.

The simulated results of the high-risk zone for fish entrainment indicate that fish are of the highest risk during low pool, as the volume of the forebay exceeding specific velocity thresholds is higher. However, many entrainment events recorded for adult bull trout through Mica dam occurred late in the year when the reservoir was at high pool and drafting (Martins et al. 2013). This history indicates that the actual entrainment of fish through hydropower turbines involves both the physical hydraulics and as well as behavioural biology, which is species specific. Indeed, fine-scale tracking of adult bull trout within 350 m of the powerhouse revealed that these fish resided for longer in the forebay and more closely approached the intakes late in the year (Martins et al. 2014). Kokanee have also been observed being entrained through Mica dam (Alf Leake, personal communication), but there is currently no data on the magnitude and seasonal patterns of entrainment.

The velocities that are generated by the intakes are relatively low when compared to the theoretical swimming ability of some species and life stages. For example, juvenile bull trout (110 to 190 mm) have mean critical swimming speeds >0.48 m/s (Mesa et al. 2004). As absolute swimming speeds are correlated with body size, adults (>300 mm) would have much greater swimming speeds than the water speeds they may experience in the Mica forebay (Scott and Crossman 1998). Smaller fish of other species such as kokanee may, however, be at risk for entrainment, as well as adult fish that are unable to detect the relatively rapid acceleration introduced by the swirling flow in the vortex core. The high-risk zones for fish entrainment at Mica include areas directly adjacent to the intakes, as well as the area adjacent to the wing wall above Intake 1 and Intake 6 based on the CFD simulation in this study. Compared to the forebay area considered as the theoretical “risk” zone in Martins et al. (2013, 2014), the actual risk zone based on this hydraulic analysis is much smaller. Fish would have to be very close to the powerhouse to experience such flows that would exceed swimming ability and presumably lead to entrainment.

These findings reveal that the entrainment risk zone is relatively small, representing the areas immediately adjacent to the intakes. Although water velocities certainly accelerate in this area, they likely do not exceed the swimming ability of larger fish species. However, smaller fish, earlier life-stages of large fish and poor swimmers may be at risk of entrainment. When the water is at low pool, and is still drafting, the velocities in the forebay are at the highest suggesting that entrainment risk varies seasonally. These observations complement those derived from parallel fish telemetry studies (i.e., Martins et al. 2013, 2014).

Conclusions

A field ADCP and CFD study was completed to evaluate the impact of dam operation on the upstream flow field and to gain insight as to the risk of fish entrainment for the forebay of Mica Dam, located on the Columbia River in BC, Canada. This study presents novel approach to collecting ADCP measurements in a reservoir environment by suspended and ADCP below and anchored boat. Additionally, a CFD model was used to simulate the forebays hydraulics and relates both fish habitat use and swimming capability to potential for entrainment risk. The study demonstrates how CFD modelling can be used to establish the

Fig. 10. Velocity magnitude profile 0, 5, 10, 25, and 50 m upstream of intake: (a) Intake 1 and (b) Intake 3. [Colour online.]

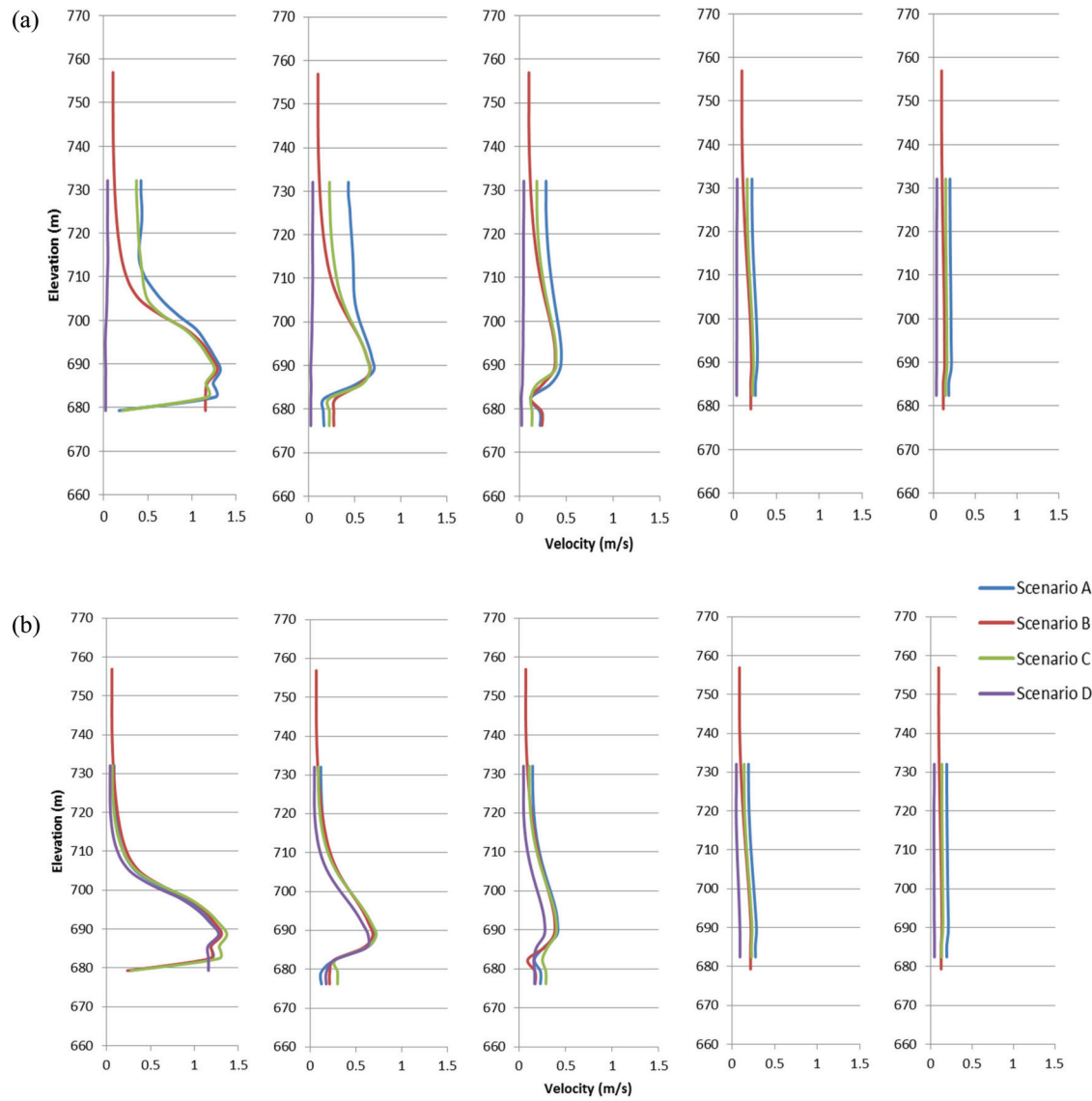


Table 2. Fish entrainment risk zone volumes.

Threshold velocity (m/s)	Scenario A (m ³)	Scenario B (m ³)	Scenario C (m ³)	Scenario D (m ³)
0.015	558481	151223	171214	6370
0.025	86833	48418	36558	2065
0.050	10171	8622	5281	19
0.100	2840	3033	1389	0

high-risk zone for fish entrainment. A potential flow solution was also applied to the flow field upstream of the facility, and shown to provide adequate results when the boundary conditions were properly represented using images of the intakes.

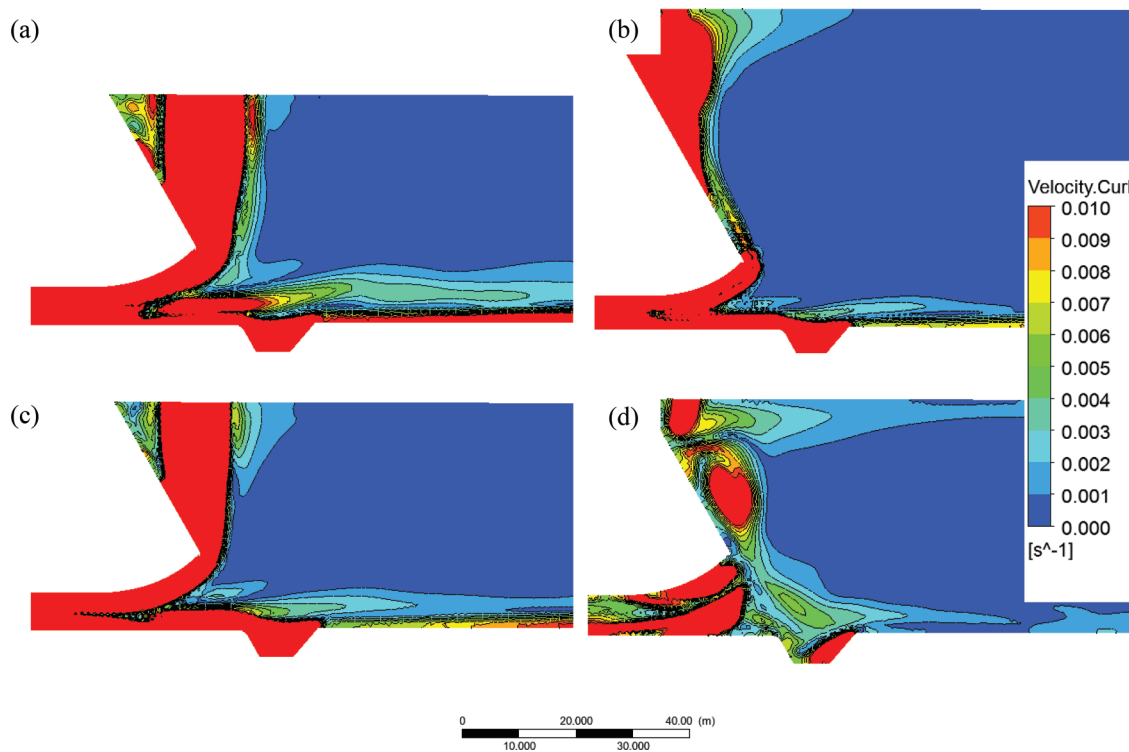
The impact of water surface elevation on the flow field was evaluated as the reservoir level of Mica Dam fluctuates greatly over the course of the year. The results indicate there is a great seasonal variation in the forebay flow field generated by the intakes. When the water is at low pool, and is drafting, the velocities in the forebay are at the highest. In these discharge scenarios there is also a consistent vortex formed above Intake 1 and

Intake 6, which generates a high velocity swirling flow at all elevations.

The intake operations also influence the flow hydraulics upstream of the dam. The velocity field that is generated by the dam shows distinct variation with depth as well as distance along the dam face for the zone within 15 m, or approximately twice the equivalent diameter of the intakes, of the dam in all operational scenarios. Peak velocities occur in front of each of the operational intakes, at the intake elevation, with reduced velocities between each intake and above the intakes' elevation. Beyond 15 m, the velocity profile becomes uniform at all depths and distances along the dam face. Within 15 m of the dam face, the flow is best represented as a series of point sinks along the dam face. Beyond this, the flow field can be represented as a line sink.

It is necessary to link fish species and fish biology in interpreting fish entrainment risk analysis. While the low water level in the spring indicates a high entrainment risk, the turbines are rarely operated during spring and bull trout (at least) rarely use the forebay at this time or they stay close to the water surface where water velocities are negligible. On the other hand, significant

Fig. 11. Velocity curl profile at Intake 1: (a) Scenario A, (b) Scenario B, (c) Scenario C, and (d) Scenario D. [Colour online.]



fish entrainment was reported in the fall season as bull trout start using the forebay more and approach the intakes. An integration of hydraulic engineering with fish biology is critical in assessing fish entrainment risk.

Acknowledgements

The authors would like to thank the late Mr. Paul Higgins of BC Hydro for providing information used in the completion of this study. We would like to thank Dr. Eduardo Martins for his valuable review of this manuscript. Additionally, we would like to thank Ms. C. Beth Robertson, Mr. Chris Krath, Mr. Pierre Bourget, and Ms. Beth Manson for assistance in the collection of field data. Funding for this research was provided by the Natural Sciences and Engineering Research Council of Canada (NSERC) and BC Hydro.

References

- Anohin, V.V., Imberger, J., Romero, J.R., and Ivey, G.N. 2006. Effect of long internal waves on the quality of water withdrawn from a stratified reservoir. *Journal of Hydraulic Engineering*, **132**(11): 1134–1145. doi:[10.1061/\(ASCE\)0733-9429\(2006\)132:11\(1134\)](https://doi.org/10.1061/(ASCE)0733-9429(2006)132:11(1134)).
- Barnthouse, L.W. 2013. Impacts of entrainment and impingement on fish populations: A review of the scientific evidence. *Environmental Science & Policy*, **31**: 149–156. doi:[10.1016/j.envsci.2013.03.001](https://doi.org/10.1016/j.envsci.2013.03.001).
- BC Hydro. 2006a. Fish entrainment risk screening and evaluation methodology. BC Hydro, Report No. E478. Burnaby, BC.
- BC Hydro. 2006b. Mica Dam Entrainment Risk Screening, BC Hydro, Report No. E487. Burnaby, BC.
- Bray, K., Sebastian, D., Weir, T., Pieters, R., Harris, S., Brandt, D., and Vidmanic, L. 2013. Kinbasket and reeve, Istoke reservoirs ecological productivity and kokanee population monitoring 2008 – 2010 Synthesis Report. BC Hydro Reference No. CLBMON-2 and CLBMON-3. Burnaby, BC.
- Bryant, D.B., Khan, A.A., and Aziz, N.M. 2008. Investigation of flow upstream of orifices. *Journal of Hydraulic Engineering*, **134**(1): 98–104. doi:[10.1061/\(ASCE\)0733-9429\(2008\)134:1\(98\)](https://doi.org/10.1061/(ASCE)0733-9429(2008)134:1(98)).
- Caliskan, A., and Elci, S. 2009. Effects of selective withdrawal on hydrodynamics of a stratified reservoir. *Water Resources Management*, **23**: 1257–1273. doi:[10.1007/s11269-008-9325-x](https://doi.org/10.1007/s11269-008-9325-x).
- Casamitjana, X., Serra, T., Colomer, J., Baserba, C., and Perez-Losada, J. 2003. Effects of the water withdrawal in the stratification patterns of a reservoir. *Hydrobiologia*, **504**(1–3): 21–28. doi:[10.1023/B:HYDR.0000008504.61773.77](https://doi.org/10.1023/B:HYDR.0000008504.61773.77).
- Coutant, C.C., and Whitney, R.R. 2000. Fish behaviour in relation to passage through hydropower turbines: a review. *Transactions of the American Fisheries Society*, **129**(2): 351–380. doi:[10.1577/1548-8659\(2000\)129<351:FBIRTP>2.0.CO;2](https://doi.org/10.1577/1548-8659(2000)129<351:FBIRTP>2.0.CO;2).
- EPRI. 1992. Fish entrainment and turbine mortality review and guidelines. Stone & Webster Environmental Service, Boston, MA.
- Fischer, H.B., List, E.J., Koh, R.C.Y., Imberger, J., and Brooks, N.H. 1979. Mixing in Reservoirs. Mixing in Inland and Coastal Waters, Academic Press Inc., San Diego, CA, pp. 150–228.
- Goodwin, R.A., Nestler, J.M., Anderson, J.J., Weber, L.J., and Loucks, D.P. 2006. Forecasting 3-D fish movement behavior using a Eulerian-Lagrangian-agent method (ELAM). *Ecological Modelling*, **192**(1–2): 197–223. doi:[10.1016/j.ecolmodel.2005.08.004](https://doi.org/10.1016/j.ecolmodel.2005.08.004).
- Goodwin, R.A. 2004. Hydrodynamics and juvenile salmon movement behavior at Lower Granite Dam: decoding the relationship using 3-D space-time (Cell Agent IBM) simulation. Ph.D. Thesis, Department of Civil and Environmental Engineering, Cornell University, Ithaca, NY.
- Huang, B., Zhu, D.Z., Shao, W., Fu, J.J., and Rui, J.L. 2015. Forebay hydraulics and fish entrainment risk assessment upstream of a high head dam in China. *Journal of Hydro-environment Research*, **9**(1): 91–103. doi:[10.1016/j.jher.2014.03.002](https://doi.org/10.1016/j.jher.2014.03.002).
- Imberger, J. 1980. Selective withdrawal: a review, 2nd Int. Symp. on Stratified Flows, IAHR, Norway, p.381.
- Islam, M., and Zhu, D.Z. 2011. Flow upstream of two-dimensional intakes. *Journal of Hydraulic Engineering*, **137**(1): 129–134. doi:[10.1061/\(ASCE\)HY.1943-7900.0000284](https://doi.org/10.1061/(ASCE)HY.1943-7900.0000284).
- Katopodis, C., and Gervais, R. 1991. Ichthyomechanics. Freshwater Institute, Central and Atlantic Region, Department of Fisheries and Oceans, Winnipeg, MB.
- Khan, L.A., Wicklein, E.A., Rashid, M., Ebner, L.L., and Richards, N.A. 2004. Computational fluid dynamics modeling of turbine intake hydraulics at a hydropower plant. *Journal of Hydraulic Research*, **42**(1): 61–69. doi:[10.1080/00221686.2004.9641184](https://doi.org/10.1080/00221686.2004.9641184).
- Langford, M., Zhu, D.Z., and Leake, A. 2015. Upstream hydraulics of a run-of-the-river hydropower facility for fish entrainment risk assessment. *Journal of Hydraulic Engineering*, **142**(4): 05015006. doi:[10.1061/\(ASCE\)HY.1943-7900.0001101](https://doi.org/10.1061/(ASCE)HY.1943-7900.0001101).
- Liermann, C.R., Nilsson, C., Robertson, J., and Ng, R.Y. 2012. Implications of dam obstruction for global freshwater fish diversity. *BioScience*, **62**(6): 539–548. doi:[10.1525/bio.2012.62.6.5](https://doi.org/10.1525/bio.2012.62.6.5).
- Marcy, B.C., Jr., Beck, A.D., and Ulanowicz, R.E. 1978. Effects and impacts of physical stress on entrained organisms. In *Power plant entrainment: a*

- biological assessment. Edited by J.R. Schubel and B.C. Marcy, Jr. Academic Press, New York, NY, pp. 135–188.
- Martins, E.G., Gutowsky, L.F.G., Harrison, P.M., Flemming, J.E., Jonsen, I.D., Zhu, D.Z., et al. 2014. Behavioral attributes of turbine entrainment risk for adult resident fish revealed by acoustic telemetry and state-space modeling. *Animal Biotelemetry*, **2**(1): 13. doi:[10.1186/2050-3385-2-13](https://doi.org/10.1186/2050-3385-2-13).
- Martins, E.G., Gutowsky, L.F.G., Harrison, P.M., Patterson, D.A., Power, M., Zhu, D.Z., et al. 2013. Forebay use and entrainment rates of resident adult fish in a large hydropower reservoir. *Aquatic Biology*, **19**(3): 253–263. doi:[10.3354/ab00536](https://doi.org/10.3354/ab00536).
- Mesa, M.G., Welland, L.K., and Zydlewski, G.B. 2004. Critical swimming speeds of wild bull trout. *Northwest Science*, **78**: 59–65.
- Meselhe, E.A., and Odgaard, A.J. 1998. 3D numerical flow model for fish diversion studies at Wanapum dam. *Journal of Hydraulic Engineering*, **124**(12): 1203–1214. doi:[10.1061/\(ASCE\)0733-9429\(1998\)124:12\(1203\)](https://doi.org/10.1061/(ASCE)0733-9429(1998)124:12(1203)).
- NPP, 2005. Fish entrainment and mortality study, Vol 1, Niagara Power Project. New York Power Authority. White Plains, NY.
- Piria, M., Simonović, P., Zanella, D., Čaleta, M., Šprem, N., Paunović, M., et al. 2019. Long-term analysis of fish assemblage structure in the middle section of the Sava River – The impact of pollution, flood protection and dam construction. *The Science of the total environment*, **651**(Pt. 1): 143–153. doi:[10.1016/j.scitotenv.2018.09.149](https://doi.org/10.1016/j.scitotenv.2018.09.149). PMID:[30227284](#).
- Potter, M.C., and Wiggert, D.C. 2002. Mechanics of fluids. 3rd Edition. Wadsworth Group A Division of Thomson Learning Inc. Pacific Grove, CA.
- Rakowski, C.L., Richmond, M.C., Serkowski, J.A., and Ebner, L. 2002. Three dimensional simulation of forebay and turbine intakes flows for the Bonneville project. Proceeding of HydroVision, Portland, OR, p. 2002.
- Schilt, C.R. 2007. Developing fish passage and protection at hydropower dams. *Applied Animal Behaviour Science*, **104**(3–4): 295–325. doi:[10.1016/j.applanim.2006.09.004](https://doi.org/10.1016/j.applanim.2006.09.004).
- Scott, W.B., and Crossman, E.J. 1998. Freshwater fishes of Canada. Galt House Publications, Oakville, ON.
- Shammaa, Y., and Zhu, D.Z. 2010. Experimental study on selective withdrawal in a two-layer reservoir using a temperature-control curtain. *ASCE Journal of Hydraulic Engineering*, **136**(4): 234–246.
- Shammaa, Y., Zhu, D.Z., and Rajaratnam, N. 2005. Flow upstream of orifices and sluice gates. *Journal of Hydraulic Engineering*, **131**(2): 127–133. doi:[10.1061/\(ASCE\)0733-9429\(2005\)131:2\(127\)](https://doi.org/10.1061/(ASCE)0733-9429(2005)131:2(127)).
- Wicklein, E.A., Khan, L.A., Rashid, M., Deering, M.K., and Nece, R.E. 2002. A three dimensional computational fluid dynamics model of the forebay of Howard Hanson dam. Washington, Proceeding, Hydro Vision 2002, Portland, OR.

List of symbols

- D depth (m)
 g gravitational acceleration (m/s^2)
 H total depth of forebay (m)
 P pressure (Pa)
 T temperature ($^\circ\text{C}$)
 u velocity in the x direction (toward the dam) (m/s)
 v velocity in the y direction (parallel the dam) (m/s)
 w velocity in the z direction (vertical) (m/s)
 ρ density (kg/m^3)
 ρ_{ref} reference density at water surface (kg/m^3)